$Zr_9Co_2P_4$ and $Zr_9Ni_2P_4$: A New 3D Structure Type, Consisting of Edge- and Vertex-Condensed Zr_6 Octahedra

Holger Kleinke and Hugo F. Franzen*

Ames Laboratory-DOE, Iowa State University, Ames, Iowa 50011

Received February 28, 1996[⊗]

The isostructural title compounds were synthesized by arc-melting of stoichiometric ratios of ZrP, Zr, and Co and Ni, respectively, and subsequent annealing at 1450 °C. Their crystal structure (space group *P*4/*mbm*; $Zr_9Co_2P_4$, $a = 12.1200(6)$ Å, $c = 3.6158(4)$ Å, $V = 531.37(7)$ Å^3, $Z = 2$; $Zr_9Ni_2P_4$, $a = 12.0862(2)$ Å, $c = 3.6435(3)$ Å, $V = 532.23(5)$ Å^3, $Z = 2$) is derived from a three-dimensional network of Zr_6 octahedra. These octahedra are connected via common vertices to form chains parallel to the *c* axis and via common edges and vertices in the *ab* plane, resulting in one double chain and one single chain. Both kinds of the interstitial atoms, the iron-group-metal atom and the phosphorus, are situated in trigonal prismatic holes between these chains, forming short M−P and M−M′ bonds. These octahedra can be described as being of the M_6X_8 cluster type as is also observed in the chalcogenide Chevrel phases. Due to the electronically nonsaturated character of the Zr octahedra and their three-dimensional connectivity, three-dimensional metallic properties are expected for both phosphides, and metallic behavior is confirmed by the observation of Pauli paramagnetism for both compounds.

Introduction

In recent decades, the metal-rich phosphides, sulfides, and selenides of the early transition metals zirconium, hafnium, niobium, and tantalum have attracted wide interest.[1,2] Despite numerous investigations in the past, several new binary compounds have recently been identified, e.g., Zr_2P,[3] Zr_7P_4,[4] Hf_2Se_3,[5] and Ta_2Se.[6] Many of these binary metal-rich phases (e.g., Ti_2S,[7] Ti_8S_3,[8] Zr_2S,[9,10] $Nb_{21}S_8$,[11] $Nb_{14}S_5$,[12] Zr_2P, Zr_7P_4, Hf_2P,[13] Nb_8P_5,[14] Nb_7P_4,[15] and Ta_2P[16]) belong to a structure family with three common features: (i) all atoms are situated on mirror planes, perpendicular to a short axis of ca. 3.6 Å, (ii) the metal sublattice contains fragments of the *bcc* packing and, therefore, condensed empty octahedral clusters, and (iii) the nonmetal atoms are surrounded by metal atoms only, usually within a (capped) trigonal prism.

In the ternary systems, consisting of the nonmetal P or S atoms and an early- and a late-transition metal, compounds with new structure types have been found to form with unusual structure motifs and features, for instance having a mixed occupation of nickel and sulfur atoms on the same atomic site[17,18] or showing unusual superconductive properties.[19] Besides numerous Zr/Hf-poor ternary phosphides in the systems (Zr/Hf)/(Fe,Co,Ni)/P, only two different Zr- or Hf-rich phosphides have been described in the literature, namely $Zr_2Ni_{0.48}P$[20] and $M_4M'P$ (M = Zr, Hf; M′ = Fe, Co, Ni).[21] The possibility of observing different behavior for ternary Zr and Hf phosphides has not systematically been investigated so far.

Our investigation of the ternary systems (Zr/Hf)/(Fe,Co,Ni)/P was initiated in order to increase the understanding of the relationships among the structure, bonding, and physical properties in such metal-rich compounds. Here we report the preparation, structure, and properties of two new isostructural zirconium phosphides that crystallize in a new structure type belonging to the structure family that contains condensed empty octahedral clusters. Under similar conditions in the Hf/Co/P system another new structure ($Hf_5Co_{1+x}P_{3-x}$[22]) was found to form. The latter structure does not contain the *bcc* units, which highlights some of the structural differences between Zr and Hf phosphides. Additionally in the Hf/Co/P compound, one crystallographic position was found to be fractionally occupied by Co and P, indicating that—at least in this case—both kinds of interstitial atoms can formally be considered as anions.

Experimental Section

Synthesis. $Zr_9Ni_2P_4$ was first observed as the main product after a reaction that involved arc-melting of a pellet of 1.429 mmol ZrP, 1.429 mmol Zr, and 0.714 mmol Ni, corresponding to the starting composition "$Zr_8Ni_2P_4$". ZrP was prepared by annealing stoichiometric amounts of Zr (Alfa, powder, −20 + 60 mesh, purity 99.7% (Hf impurity: 97 ppm)) and P (Alfa, powder, −100 mesh, red amorphous, 99%) in an evacuated silica tube at 800 °C over a period of 5 days; Ni has been obtained from Fisher in form of a purified powder, and Co, from Alfa (powder, −50 + 150 mesh, 99.9%). Once the stoichiometry had been determined from X-ray single crystal structure analysis, $Zr_9Co_2P_4$ and $Zr_9Ni_2P_4$ were prepared as single phases, starting from the stoichiometric

[⊗] Abstract published in *Advance ACS Abstracts,* August 15, 1996.

(1) Franzen, H. F. *Prog. Solid State Chem.* **1978**, *12*, 1.
(2) Marking, G. A.; Franzen, H. F. *J. Alloys Compd.* **1994**, *204*, L17.
(3) Ahlzén, P.-J.; Rundqvist, S. *Z. Kristallogr.* **1989**, *189*, 117.
(4) Ahlzén, P.-J.; Rundqvist, S. *Z. Kristallogr.* **1989**, *189*, 149.
(5) Schewe-Miller, I. M.; Young, V. G., Jr. *J. Alloys Compd.* **1994**, *216*, 113.
(6) Harbrecht, B. *Angew. Chem., Int. Ed. Engl.* **1989**, *28*, 1660.
(7) Owens, J. P.; Conard, B. R.; Franzen, H. F. *Acta Crystallogr.* **1967**, *23*, 77.
(8) Owens, J. P.; Franzen, H. F. *Acta Crystallogr.* **1974**, *B30*, 427.
(9) Conard, B. R.; Franzen, H. F. *High Temp. Sci.* **1971**, *3*, 49.
(10) Yao, X.; Franzen, H. F. *J. Less-Common Met.* **1988**, *142*, L27.
(11) Franzen, H. F.; Beinecke, T. A.; Conard, B. R. *Acta Crystallogr.* **1968**, *B24*, 412.
(12) Chen, H.-Y.; Tuenge, R. T.; Franzen, H. F. *Inorg. Chem.* **1973**, *12*, 552.
(13) Lundström, T.; Ersson, N.-O. *Acta Chem. Scand.* **1968**, *22*, 1801.
(14) Anugul, S.; Pontchour, C.; Rundqvist, S. *Acta Chem. Scand.* **1963**, *17*, 26.
(15) Rundqvist, S. *Acta Chem. Scand.* **1966**, *20*, 2427.
(16) Nylund, A. *Acta Chem. Scand.* **1966**, *20*, 2393.
(17) Harbrecht, B. *Z. Kristallogr.* **1988**, *182*, 118.
(18) Mackay, R.; Franzen, H. F. *Z. Anorg. Allg. Chem.* **1992**, *616*, 154.
(19) Marking, G. A.; Franzen, H. F.; Ostenson, J. E.; Ling, M. M.; Finnemore, D. K.; Laabs, F. C. *Phys. Rev. B* **1993**, *48*, 16630.
(20) Bruskov, V. A.; Lomnitskaya, Y. F.; Kuz'ma, Y. B. *Sov. Phys. Crystallogr.* **1988**, *33* (2), 199.
(21) Lomnitskaya, Y. F.; Kuz'ma, Y. B. *Inorg. Mater. Transl. (Neorg. Mater.)* **1980**, *16* (6), 705.
(22) Kleinke, H.; Franzen, H. F. *J. Alloys Compds.* **1996**, *238*, 68.

S0020-1669(96)00214-5 CCC: $12.00

Table 1. Selected Crystallographic Data for $Zr_9Ni_2P_4$

empirical formula	$Zr_9Ni_2P_4$
M_r	1062.28
temp of data collcn	295 K
cryst dimens	0.05 mm × 0.01 mm × 0.006 mm
space group	*P*4/*mbm* (No. 127)
unit cell dimens	$a = 12.0862$ (2) Å, $c = 3.6435$ (3) Å, $V = 532.23(5)$ Å^3
no. of formula units per cell	2
calcd density	6.628 g/cm^3
abs coeff	12.32 mm^{-1}
F(000)	952
scan mode, scan width	$\omega-2\theta$, $(1.78 + 0.34 \tan\theta)°$
scan speed	8.0°/min (in ω, max 3 rescans)
range of 2θ	3−60°
no. of measd reflcns	3247
no. of indepdt reflcns	513 ($R_{int} = 0.077$)
no. of obsd reflcns ($I > 3.0\sigma(I)$)	328
no. of params refined	28
R,[a] R_w,[b] goodness of fit (GOF[c])	0.025, 0.022, 1.419

[a] $R = \sum||F_o| - |F_c||/\sum|F_o|$. [b] $R_w = [\sum w(|F_o| - |F_c|)^2/\sum w(F_o)^2]^{1/2}$; $w = \sigma_F^{-2}$. [c] GOF $= \sum(||F_o| - |F_c||/\sigma_i)/(N_{observns} - N_{params})$.

ratios of ZrP, Zr, and Co and Ni, respectively. These mixtures were pressed to pellets under a pressure of 10 000 psi and then arc-melted twice for 20 s under an argon atmosphere. After arc-melting, the samples were put on a Zr foil and into a tungsten crucible. The melted ingots were annealed in an induction furnace under a dynamic vacuum (10^{-6} Torr) over a period of 6 h at a temperature of 1450 °C. X-ray powder diffraction data were obtained with a Guinier FR552 camera (Enraf-Nonius) using Cu Kα radiation ($\lambda = 1.5406$ Å) and silicon powder as an internal standard. The powder diagrams of the products contained only the reflections of $Zr_9Co_2P_4$ and $Zr_9Ni_2P_4$, respectively, indicating a homogeneous reaction product. Indexing of the powder diagrams of the bulk samples on the basis of tetragonal symmetry yielded final lattice constants of $a = 12.1200(6)$ Å, $c = 3.6158(4)$ Å, and $V = 531.37(7)$ Å^3 for $Zr_9Co_2P_4$ and $a = 12.0862(2)$ Å, $c = 3.6435$-(3) Å, and $V = 532.23(5)$ Å^3 for $Zr_9Ni_2P_4$.

Electron Dispersive Spectroscopy (EDS). To check for adventitious impurities, i.e., W, $Zr_9Co_2P_4$ and $Zr_9Ni_2P_4$ crystals were scanned using a JSM-840A scanning microscope (JEOL). No impurities were found. Using the standardless EDS analysis, the composition of the crystals was determined to be homogeneous within the range of the standard deviations of about ±10% for each element, which can be explained by the different orientations of the scanned surfaces.

Structure Determination. A needlelike single crystal isolated from a sample with the starting composition "Zr_4NiP_2", and having the approximate dimensions of 0.05 mm × 0.01 mm × 0.006 mm, was selected for data collection and then mounted on a glass fiber. The crystal quality was checked with a Weissenberg camera. The data were collected using a Rigaku AFC6R diffractometer equipped with graphite monochromated Mo Kα radiation and a 12 kw rotating anode. The orientation matrix for the data collection and the preliminary cell constants were obtained from a least-squares refinement using 25 carefully centered reflections in the range $14.73° < 2\theta < 36.64°$. The tetragonal symmetry, indicated by the cell dimensions, was checked by scanning 20 symmetry equivalent reflections. The ideal tetragonal lattice constants were refined to $a = 12.098(3)$ Å, $c = 3.6293(9)$ Å, and $V = 531.2(2)$ Å^3. Four octants were measured using the $\omega-2\theta$ technique to a maximum 2θ value of 60° and later merged. The intensities of three standard reflections, measured after every 150 reflections, remained constant throughout data collection. The data were corrected for Lorentz and polarization effects.

Since the distribution of the normalized structure factors pointed to a centrosymmetric space group, and because of the observed systematic extinction of $k = 2n + 1$ for all 0*kl* reflections, the space group was determined to be *P*4/*mbm* (No. 127). The structure was solved by direct methods, using the SHELXS-86 program package.[23] The four strongest peaks, taken from the *E*-map, were identified as Zr positions. Two further positions, taken from the following difference Fourier analysis (calculated with the TEXSAN program package[24]), were identified as one Ni and one P site, corresponding to their heights. The crystallographic data for $Zr_9Ni_2P_4$ are summarized in Table 1; the atomic positions and the equivalent temperature factors may be found in Table 2. The anisotropic temperature factors are contained in the Supporting Information.

Table 2. Atomic Positions and Equivalent Temperature Factors for $Zr_9Ni_2P_4$

atom	site	*x*	*y*	*z*	B_{eq}[a]/Å^2
Zr(1)	2*a*	0	0	0	0.45(3)
Zr(2)	8*j*	0.182 19(6)	0.102 45(6)	1/2	0.51(3)
Zr(3)	4*g*	0.405 86(6)	0.0941 4(6)	0	0.83(2)
Zr(4)	4*g*	0.121 23(7)	0.378 77(7)	1/2	0.77(2)
Ni	4*g*	0.246 2(1)	0.253 8(1)	0	0.99(3)
P	8*i*	0.056 3(2)	0.223 8(2)	0	0.43(7)

[a] $B_{eq} = (8\pi^2/3)\sum_i\sum_j U_{ij} a_i^* a_j^* \vec{a}_i \vec{a}_j$.

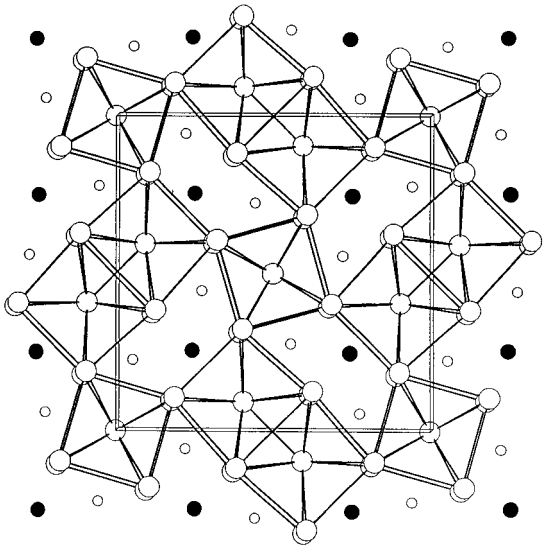

Figure 1. Structure of $Zr_9Ni_2P_4$ in a projection along [001], emphasizing the cubic Zr units: small, white circles, P; medium, black circles, Ni; large, white circles, Zr.

Magnetic Susceptibilities. Magnetic data were obtained for both compounds, $Zr_9Co_2P_4$ and $Zr_9Ni_2P_4$, from a ca. 25 mg bulk sample. Temperature-dependent measurements were made at 3 T in the temperature range 5−300 K on a Quantum Design MPMS SQUID magnetometer. The data were corrected for the diamagnetic atom cores. The field dependence was checked at 20 K between 0 and 5.4 T.

Results and Discussion

The new compounds $Zr_9Co_2P_4$ and $Zr_9Ni_2P_4$ are isostructural, as can be seen in their nearly identical powder diagrams and cell dimensions. Since the single-crystal structure determination has been done only on $Zr_9Ni_2P_4$, the discussion will refer mainly to this compound. The crystal structure of $Zr_9Ni_2P_4$ is shown Figure 1.

Two different fragments of the *bcc* packing occur in the structure of $Zr_9Ni_2P_4$: first, there are centered cubes, situated at the origin and at the center of the unit cell, which are condensed via opposite faces to linear chains parallel to the crystallographic *c* axis, and second, there are two cubes within the unit cell, sharing one face to form a double unit, which are connected in the same way to a linear double chain of centered cubes, again running parallel to [001]. As depicted in Figure 1, which emphasizes the cubic units, these two fragments are

(23) Sheldrick, G. M. SHELXS-86, Universität Göttingen, Germany, 1986.

(24) TEXSAN: *Single Crystal Structure Analysis Software, Version 5.0*; Molecular Structure Corp.: The Woodlands, TX, 1989.

Table 3. Parameters Used in the EH Calculations

orbital	H_{ii}/eV	ζ_1	c_1	ζ_2	c_2
Zr, 5s	−8.93	1.820			
Zr, 4p	−5.29	1.780			
Zr, 4d	−9.24	3.840	0.6213	1.505	0.5798
Ni, 4s	−8.62	1.925			
Ni, 4p	−4.28	1.925			
Ni, 3d	−11.06	5.750	0.5862	2.200	0.5845
P, 3s	−18.60	1.880			
P, 3p	−12.50	1.630			

connected via common vertices to a three-dimensional network. These units are formed by the four crystallographically different Zr atoms.

The smaller metal atom Ni, as well as the nonmetal atom P, is situated in capped trigonal prismatic voids of the Zr sublattice. These trigonal prisms are connected via their opposite triangular faces to chains parallel [001]. The trigonal Zr_6Ni prisms are capped by the Zr(3) atom of the center of the double cube chain and by two P atoms, resulting in a three-capped trigonal prismatic coordination for the Ni atom. The Zr_6Ni prism is quite regular, with Zr−Ni distances between 2.6951(8) Å and 2.807(2) Å. Including the Zr−Ni bond across a rectangular face of the prism of 2.729(2) Å, a mean Zr−Ni distance of 2.732 Å is calculated. In the only other reported phosphide ($Zr_2Ni_{0.48}P$[20]) with Ni located in the center of a trigonal Zr_6 prism, slightly shorter Zr−Ni distances, with mean distances of 2.642 Å for the 6-fold Zr-coordinated Ni and 2.709 Å for the Ni atom in the singly-capped prism, were observed.

Trigonal prismatic Zr coordination is expected for metal-rich phosphides, as comparisons with other, previously found phosphides show. Similar distances within those prisms have been observed in other systems, namely 2.7871(8) Å for the six Hf−Ni distances in $HfNi_xP$,[25] 2.789 Å for the six Hf−Co distances in the Hf_6Co prism of $Hf_2Co_4P_3$,[26] and 2.677 Å for the mean Hf−Co distance in the singly-capped Hf_6Co prism of $Hf_5Co_{1+x}P_{3-x}$.[22] Presumably all these distances have bonding character, compared with the sum of the Pauling radii, i.e., $r_{Zr} + r_{Ni} = 1.454$ Å + 1.154 Å = 2.608 Å.[27] Using the concept of Lewis acids and bases, the bonding occurs between an electron-poor metal (Zr/Hf), considered as the acid, and an electron-rich metal (Fe/Co/Ni) as the base.

To confirm the bonding character, we calculated the Mulliken overlap populations (MOP), using the extended-Hückel method.[28,29] The parameters used for Zr were obtained from solid-state charge iterations on Zr_7P_4, and the parameters for P were taken from the literature.[30] The Ni parameters were optimized by charge iteration on $Zr_9Ni_2P_4$ with given Zr and P parameters (see Table 3). According to our considerations, the calculated Mulliken overlap populations for the Zr−Ni bonds of $Zr_9Ni_2P_4$ are all positive (ranging from 0.063 to 0.208, as depicted in Table 4), as expected after evaluation of the Pauling bond orders $d(n) = d(1) - 0.6 \log n$ (PBO's from 0.46 to 0.72). The mean Ni−Zr MOP of 0.13 is comparable to the mean Fe−Zr MOP in the structure of $Zr_6I_{14}Fe$[31] (0.16) with definitely bonding Fe−Zr interaction, Fe situated in the center of a Zr_6 octahedron. Thus, the Zr−Ni interactions are presumed to have bonding character, also.

Table 4. Selected Interatomic Distances (Å), PBO,[a] and MOP[b] for $Zr_9Ni_2P_4$

central atom	neighbors	dist	PBO	MOP
Zr(1)	2 Zr(1)	3.6435(3)	0.06	0.093
	8 Zr(2)	3.1146(6)	0.45	0.144
	4 P	2.790(2)	0.41	0.229
Zr(2)	2 Zr(1)	3.1146(6)	0.45	0.144
	2 Zr(2)	3.573(1)	0.08	0.050
	2 Zr(2)	3.6435(3)	0.06	0.042
	1 Zr(2)	3.681(2)	0.05	0.124
	2 Zr(3)	3.2614(9)	0.26	0.167
	1 Zr(4)	3.420(1)	0.14	0.110
	1 Zr(4)	3.5992(7)	0.07	0.062
	2 Ni	2.6951(8)	0.72	0.132
	2 P	2.693(2)	0.58	0.211
	2 P	2.791(2)	0.41	0.222
Zr(3)	4 Zr(2)	3.2614(9)	0.26	0.167
	1 Zr(3)	3.218(2)	0.31	0.176
	2 Zr(3)	3.6435(3)	0.06	0.099
	4 Zr(4)	3.1940(9)	0.33	0.168
	1 Ni	2.729(2)	0.63	0.208
	2 P	2.854(2)	0.31	0.192
Zr(4)	2 Zr(2)	3.420(1)	0.14	0.110
	2 Zr(2)	3.5992(7)	0.07	0.062
	4 Zr(3)	3.1940(9)	0.33	0.168
	2 Zr(4)	3.6435(3)	0.06	0.042
	1 Zr(4)	4.144(2)	0.01	0.023
	2 Ni	2.807(2)	0.46	0.063
	4 P	2.728(1)	0.51	0.247
Ni	4 Zr(2)	2.6951(8)	0.72	0.132
	1 Zr(3)	2.729(2)	0.63	0.208
	2 Zr(4)	2.807(2)	0.46	0.063
	2 P	2.324(2)	0.77	0.172
P	1 Zr(1)	2.790(2)	0.41	0.229
	2 Zr(2)	2.693(2)	0.58	0.211
	2 Zr(2)	2.791(2)	0.41	0.222
	1 Zr(3)	2.854(2)	0.31	0.192
	2 Zr(4)	2.728(1)	0.51	0.247
	1 Ni	2.324(2)	0.77	0.172

[a] PBO = Pauling bond order. [b] MOP = Mulliken overlap population.

Similar structure motifs can also be found in the Ta/M′/S (M′ = Fe, Co, Ni) system. In the structure of $Ta_9M'_2S_6$,[32] M′ is found in a three-capped trigonal Ta prism with significantly shorter M−M′ bonds (M = early transition metal), due in part to the smaller M atom ($r_{Ta} = 1.343$ Å; distances within the prism, $d_{Ta-Ni} = 2.495(1)$ Å; distances to the capping Ta atoms, $d_{Ta-Ni} = 2.961(1)$ Å). Therefore, shorter Ni−Ni distances of 3.367(1) Å are found and so a pairing of the iron-group-metal atoms with significant bonding interactions is possible. This is observed in the structures of $Ta_9Fe_2S_6$ and $Ta_9Co_2S_6$, where a superstructure with alternating short and long M′−M′ distances ($d_{Fe-Fe} = 2.881(8)$ and 3.702(8) Å, $d_{Co-Co} = 2.904(6)$ and 3.670(6) Å) is found.[33] A corresponding structure distortion did not take place in the structure of $Zr_9Co_2P_4$ because the main driving force for building Co_2 pairs, as in $Ta_9Co_2S_6$,[34] is not possible through an analogous distortion, starting from the long Co−Co distance of 3.6158(4) Å in the undistorted structure.

The coordination sphere of the P atom in $Zr_9Ni_2P_4$ can be described as a trigonal prism where the rectangular faces of the Zr_6P prism are capped by one Ni and two Zr atoms (Zr(1) and Zr(3)) and the triangular faces by two P atoms at the nonbonding distance of 3.6435(3) Å, which is the shortest P−P contact in this structure. As predicted for metal-rich phosphides, all P atoms are well separated from each other. The Ni−P distance

(25) Kleinke, H.; Franzen, H. F. *Z. anorg. allg. Chem.*, in press.
(26) Ganglberger, E. *Monatsh. Chem.* **1968**, *99*, 566.
(27) Pauling, L. *The Nature of the Chemical Bond*, 3rd ed.; Cornell University Press: Ithaca, NY, 1948.
(28) Hoffmann, R. *J. Chem. Phys.* **1963**, *39*, 1397.
(29) Whangbo, M.-H.; Hoffmann, R. *J. Am. Chem. Soc.* **1978**, *100*, 6093.
(30) Clementi, E.; Roetti, C. *At. Nucl. Data Tables* **1974**, *14*, 177.
(31) Hughbanks, T.; Rosenthal, G.; Corbett, J. D. *J. Am. Chem. Soc.* **1988**, *110*, 1511.
(32) Harbrecht, B.; Franzen, H. F. *J. Less-Common Met.* **1986**, *115*, 177.
(33) Harbrecht, B. *J. Less-Common Met.* **1986**, *124*, 125.
(34) Calhorda, M. J.; Hoffmann, R. *Inorg. Chem.* **1988**, *27*, 4679.

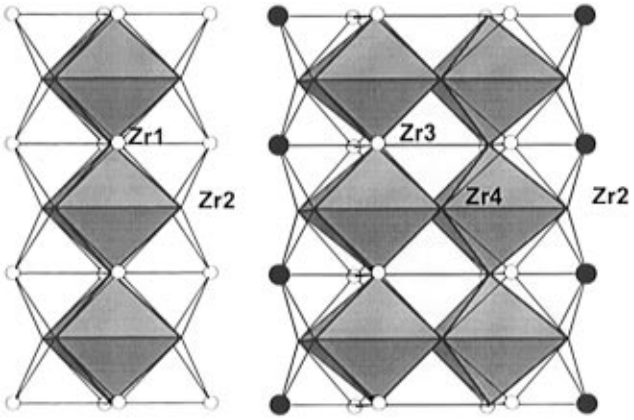

Figure 2. Chains of Zr_6 octahedra (left) and of Zr_{10} double octahedra (right): small, white circles, P; medium, black circles, Ni.

of 2.324(2) Å is slightly elongated in comparison to the sum of the Pauling radii of 2.264 Å. This points to a strong bonding character, as indicated by the calculated Pauling bond order of 0.77 and the Mulliken overlap population of 0.172, although significantly shorter Ni−P bonds have been observed in the structures of Ni_2P (2.209 Å[35]) and $HfNi_xP$ (2.1578(7) Å[25]). The length of the Ni−P bond might, to some extent, be determined by a Zr matrix effect. The Zr−P distances, occurring between the most electropositive (Zr) and the most electronegative (P) atoms, have bonding character as well, as can be seen by the Pauling bond orders (between 0.31 and 0.58) and by the overlap populations (from 0.192 to 0.247). The mean Zr−P distance of 2.759 Å is comparable to those observed in Zr_2P,[3] ranging from 2.661 Å for the monocapped Zr_6P prism to 2.793 Å for a three-capped Zr_6P prism.

For the Zr sublattice, the P and Ni atoms cap the Zr-centered Zr cubes. Only P atoms cap the single cube chain, whereas the cubes of the double chain are capped by both Ni and P. The structural fragment composed of a single chain of capped cubes, "Zr_5P_4", corresponds to the chains seen in the Ti_5Te_4 structure type,[36] whereas the fused double chain occurs in the structure of Zr_2P, too, which also contains the "Zr_5P_4" fragments.[3]

These chains of centered cubes may also be considered as chains of vertex-condensed octahedra. Since the smaller atoms cap the triangular faces of these octahedra, they may be considered as condensed M_6X_8 units, which are well−known in the Chevrel phases.[37] The concept of using condensed cluster units for describing the Ti_5Te_4 and related structure types was also discussed by Simon.[38] In the structure of $Zr_9Ni_2P_4$, nonmetal (P) and—more unusually—metal (Ni) atoms correspond to the X atoms of the condensed M_6X_8 units. The octahedral chains are emphasized in Figure 2.

Both kinds of Zr_6X_8 octahedra—the Zr_6P_8 octahedron of the single chain as well as the more condensed unit $Zr_{10}Ni_4P_8$—are constricted along the [001] direction, resulting in a short contact of 3.6435(3) Å (corresponding to the *c* axis) between the apical Zr atoms. This is comparable to the distances within the equatorial plane: in the octahedra of the single chain $Zr(2)_4Zr(1)P_4$, the basal Zr(2)−Zr(2) distance of 3.573(1) Å is about 2% shorter, whereas the mean distance of the equatorial Zr−Zr contacts within the Zr octahedra of the double chain is significantly longer with d = 3.700 Å ($d_{Zr(2)-Zr(2)}$ = 3.681(2) Å, 2x; $d_{Zr(2)-Zr(4)}$ = 3.5992(7) Å, 4x; $d_{Zr(4)-Zr(4)}$ = 4.144(2) Å).

The shortest Zr−Zr bonds occur between the apical and equatorial atoms of the octahedra ($d_{Zr(1)-Zr(2)}$ = 3.1146(6) Å in the single chain, and $d_{Zr(3)-Zr(4)}$ = 3.1940(9) Å and $d_{Zr(2)-Zr(3)}$ = 3.2614(9) Å in the double chain) and on the other hand between the neighboring vertices of the double units ($d_{Zr(3)-Zr(3)}$ = 3.218(2) Å). For these reasons, a consideration of the cluster units as centered (distorted) cubes is more useful. Whereas the $Zr(2)_8Zr(1)$ cube is almost undistorted, with all angles equal to 90° and two edges having only slightly different lengths (3.573(1) and 3.6435(3) Å), the more condensed "cubes" of the double chain are more irregular with different lengths of the edges from 3.5992(7) to 4.144(2) Å.

Similar structure motifs have been found in the structures of Zr_2P,[3] $Zr_{14}P_9$,[39] and Zr_7P_4.[4] Only Zr_2P contains the "fused" cubes as well as the "single" cubes, whereas the more P-rich $Zr_{14}P_9$ and Zr_7P_4 only consist of the single (centered) Zr cubes. In all of these three binary structures, the cubes are condensed via opposite faces to form linear chains, as it is found in the structure of $Zr_9Ni_2P_4$. The short lengths of the corresponding crystallographic axes (from 3.6049(3) to 3.6742(3) Å) point to cubic rather than octahedral arrangements, and the bonds from the centers to the corners of the single cubes are significantly shorter than those between the corners (varying from 2.995(2) to 3.324(3) Å vs from 3.375(4) to 3.703 Å). The two different fused cubes of Zr_2P both show the expansion of the Zr−Zr distance across the bond between the centers (4.130 and 4.395 Å, respectively). Therefore, a reasonable explanation for the elongation would be that the realization of a short contact between the centers leads to an increase of the crossing Zr−Zr bond length for steric reasons.

The Zr(2)−Zr(4) distance of 3.420(1) Å, occurring between the cluster units of $Zr_9Ni_2P_4$, is even shorter than the lengths of the edges of the cubic units. The fact that the overlap populations for the bonds between the centers of the cubes (apices of the octahedra) along the chain direction are significantly positive and larger than those between the corners (0.093 and 0.097 vs 0.040 and 0.038) argues against the consideration of the Zr sublattice as being constructed of simple cluster units. For all these reasons, the concept of condensed cubic or octahedral cluster units should not be pushed too far, but it is nevertheless a useful aid.

As expected for a long bond of 4.144(2) Å, the calculated MOP for the Zr(4)−Zr(4) distance, which is perpendicular to the Zr(3)−Zr(3) bond within the doubled cluster unit, is very small (0.023). In addition, the other Zr−Zr interactions within the equatorial planes also have only small overlap populations, varying from 0.050 to 0.124, compared to the Zr(2)−Zr(4) bond (MOP = 0.110) between the cubic units. Stronger Zr−Zr bonds occur between the centers of the fused cubes ($MOP_{Zr(3)-Zr(3)}$ = 0.176) and between the centers and the corners of both different cubes (MOP's (ranging from 0.144 to 0.168).

Taking all Zr−Zr <4.2 Å, Zr−Ni <3.5 Å and Zr−P distances <3.5 Å into account, various coordination numbers (CN) result for the different Zr atoms: Zr(1) is surrounded by ten Zr and four P atoms (CN = 14), Zr(2) by eleven Zr, two Ni, and four P atoms (CN = 17), Zr(3) by eleven Zr, two Ni, and two P (CN = 15), and Zr(4) by eleven Zr, two Ni, and four P atoms (CN = 17). Weighing these distances according to the Pauling bond orders, the total bond orders are still different, ranging from 4.04 (for Zr(3)) to 5.38 (for Zr(2)), with different Zr−Zr bond orders from 1.87 (Zr(4)) to 3.72 (Zr(1)). On the other

(35) Rundqvist, S. *Acta Chem. Scand.* **1962**, *16*, 992.
(36) Grønvold, F.; Kjekshus, A.; Raaum, F. *Acta Crystallogr.* **1961**, *14*, 930.
(37) Kepert, D. L. *The Early Transition Metals*; Academic Press: New York, 1972; Chapter 4.
(38) Simon, A. *Angew. Chem., Int. Ed. Engl.* **1981**, *20*, 1.
(39) Tergenius, L.-E.; Noläng, B. I.; Lundström, T. *Acta Chem. Scand.* **1981**, *A35*, 693.

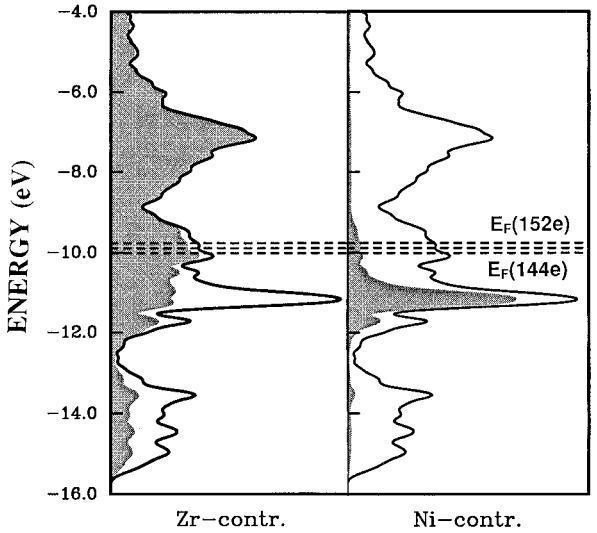

Figure 3. Density of states for $Zr_9Ni_2P_4$.

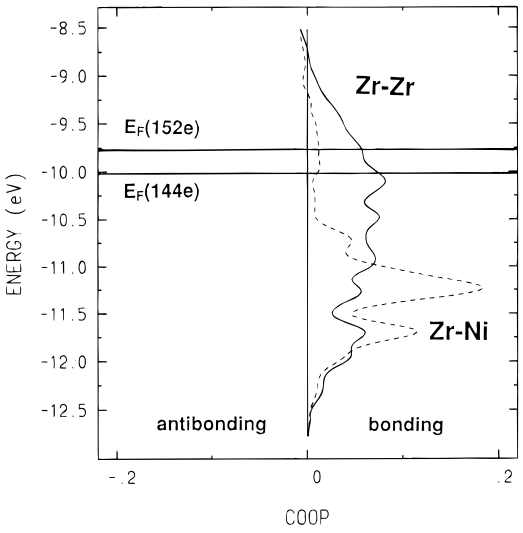

Figure 4. Selected crystal orbital overlap populations for $Zr_9Ni_2P_4$.

hand, the extended-Hückel calculations lead to similar sums of the MOP's, varying only from 2.232 to 2.306 for the four crystallographically different Zr atoms. As has been shown for $Hf_{5.08}Mo_{0.92}P_3$[40] and for metal-rich Ta sulfides,[41] the sum of the MOP is a value capable of pointing out differences or similarities of different metal sites. In this case, the differences between the metal sites are therefore not very strong. On the other hand, the sum of the Zr−Zr MOP's for the different Zr sites differ significantly from 1.040 (Zr(2)) to 1.714 (Zr(4)).

A complete replacement of Zr by the homologous Hf has failed so far. In the Hf/M′/P system loading the 9-2-4 stoichiometry yielded an unknown structure. These compounds are assumed to have more Hf−Hf contacts, according to the general conclusion, and the 5d metal prefers structures with higher metal−metal bond orders, due to the larger extension of the 5d orbitals.[42] According to the concept of Brewer−Engel,[43] Hf utilizes more s and p electrons than Zr and prefers positions with more M−M interactions for the same reason. Thus, a partial substitution of Zr by Hf might show a preference of Hf for the Zr(3) position which has the highest total Zr−Zr MOP. These investigations are currently in progress.

(40) Cheng, J.; Franzen, H. F. *J. Solid State Chem.* **1996**, *121*, 362.
(41) Köckerling, M.; Franzen, H. F. *Croat. Chim. Acta* **1995**, *68*, 709.
(42) Franzen, H. F.; Köckerling, M. *Prog. Solid State* **1995**, *23*, 265.
(43) Brewer, L. In *Alloying*; Walter, J. L., Jackson, M. R., Sims, C. T., Eds.; ASM International: Metal Park, OH, 1988; Chapter 1.

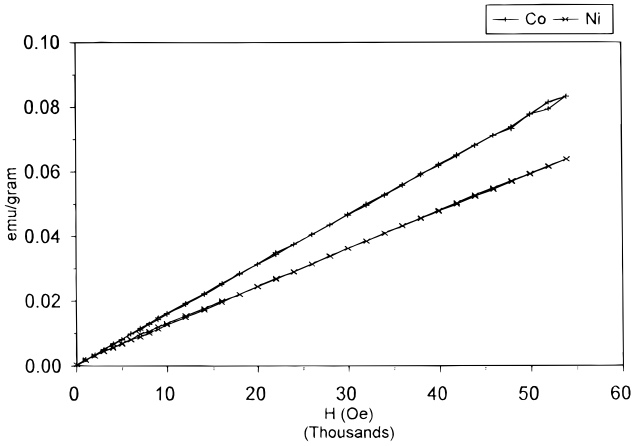

Figure 5. Field dependence of the magnetic moments of $Zr_9M'_2P_4$ at 20 K.

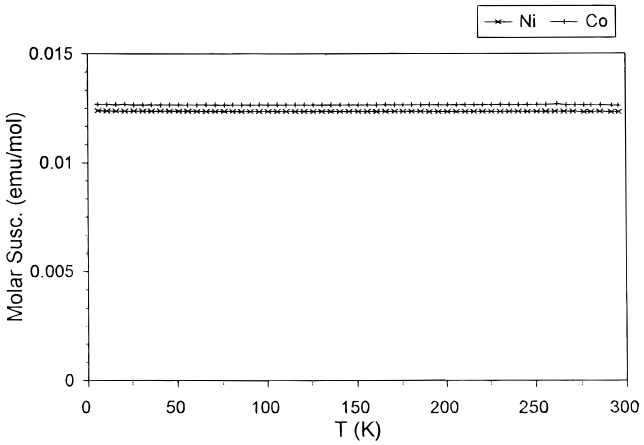

Figure 6. Temperature dependence of the magnetic susceptibility of $Zr_9M'_2P_4$ at 5 T.

Figure 3 shows the calculated density of states (DOS) for $Zr_9Ni_2P_4$ (152 electrons per unit cell), including the Fermi levels for $Zr_9Co_2P_4$ (148 electrons) and hypothetical "$Zr_9Fe_2P_4$" (144 electrons) with the parameters of $Zr_9Ni_2P_4$. As shown in Figure 3, there is a significant density of states for $Zr_9Co_2P_4$ as well as $Zr_9Ni_2P_4$ at the Fermi level, which is a little bit higher for $Zr_9Co_2P_4$ than for $Zr_9Ni_2P_4$. The main contribution to this rise comes from the Zr d orbitals. The iron-group-metal d states are located in a small region ca. 1 eV below the Fermi level, and the phosphorus 3p states lie more than 4 eV below the Fermi level. Thus, P is considered to have filled 3s and 3p states and, therefore, to have the formal oxidation state of −3. A determination of the oxidation states of the metal atoms is more complicated, because neither the Zr nor the Ni d orbitals are completely filled. Assuming reasonable oxidation states of +4 for Zr and +2 for Ni, the resulting formula of $(Zr^{4+})_9(Ni^{2+})_2(P^{3-})_4(e^-)_{28}$ shows many electrons available for delocalized metal−metal bonds. Due to the three-dimensional Zr network, metallic conductivity along all directions is expected.

To date, we have not been able to prepare "$Zr_9Fe_2P_4$". This may be seen in the differences between the electronic structure of $Zr_9Ni_2P_4$ with 152 electrons and hypothetical "$Zr_9Fe_2P_4$" with 144 electrons. The changes in the DOS curves are marginal but not the changes in the COOP (crystal orbital overlap population) curves: since phosphorus does not contribute many states to the DOS at the Fermi level of $Zr_9Ni_2P_4$, the important interactions at this energy level are the Zr−Zr, Zr−M′, and M′−M′ interactions (with M′ = Fe, Co, Ni). The M′-M′ interactions are determined to be almost zero, so we concentrate on the Zr−Zr and Zr−M′ overlap populations. If the Fermi level is

lowered, corresponding to the lower number of electrons of hypothetical "$Zr_9Fe_2P_4$", the Zr−Zr and the Zr−M′ interactions become less bonding (Figure 4). This loss in bonding energy might be the cause for the nonstability of "$Zr_9Fe_2P_4$" relatively to other phases.

In order to show the metallic behavior of $Zr_9M'_2P_4$ and to investigate the differences between $Zr_9Co_2P_4$ and $Zr_9Ni_2P_4$, the magnetic moments at 3 T between 5 and 300 K for the bulk samples of $Zr_9Co_2P_4$ and $Zr_9Ni_2P_4$ were measured. The susceptibilities obtained were corrected for the diamagnetic cores. The absence of ferromagnetic impurities (unreacted Co or Ni) was proved by field-dependent measurements at a temperature of 20 K (Figure 5): no hysteresis has been observed, and the linear increase of the magnetic moments does not correspond to ferromagnetic behavior. Both compounds show almost temperature-independent Pauli paramagnetism (Figure 6), according to the metallic properties, predicted by simple electronic considerations and by the EH calculations. Since the observed paramagnetism is almost independent from the temperature in both cases, $Zr_9Co_2P_4$ and $Zr_9Ni_2P_4$, no magnetic moments are localized on the Co or Ni sites. The higher magnetic susceptibility of $Zr_9Co_2P_4$ points to the presence of more electrons at the Fermi level, according to the calculated higher density of states at the Fermi level of $Zr_9Co_2P_4$ in comparison to $Zr_9Ni_2P_4$.

Altogether, the intuitive postulate of metallic conductivity for $Zr_9M'_2P_4$ could be confirmed by extended-Hückel calculations as well as by the experimentally determined Pauli paramagnetism. The fact, that we have been unable to substitute Zr by Hf is another example for the different behavior of Zr and Hf in metal-rich compounds. Further investigations might explain the preference of Hf for alternative structures.

Acknowledgment. H.K. thanks the Deutsche Forschungsgemeinschaft for financial support of this work. The Ames Laboratory is operated for the U.S. Department of Energy by Iowa State University under Contract No. W-7405-Eng-82. This research was also supported by the Office of the Basic Energy Sciences, Materials Science Division, Department of Energy.

Supporting Information Available: A table of anisotropic thermal parameters for $Zr_9Ni_2P_4$ (1 page). Ordering information is given on any current masthead page.

IC960214A